ACS OMEGA

Open Access

http://pubs.acs.org/journal/acsodf

Article

Micropatterned Nanofiber Scaffolds of Salmon Gelatin, Chitosan, and Poly(vinyl alcohol) for Muscle Tissue Engineering

María I. Taborda, Karina N. Catalan, Nicole Orellana, Dragica Bezjak, Javier Enrione, Cristian A. Acevedo,* and Tomas P. Corrales*

Cite This: *ACS Omega* 2023, 8, 47883−47896

Read Online

ACCESS | Metrics & More | Article Recommendations | Supporting Information

ABSTRACT: The development of scaffolds that mimic the aligned fibrous texture of the extracellular matrix has become an important requirement in muscle tissue engineering. Electrospinning is a widely used technique to fabricate biomimetic scaffolds. Therefore, a biopolymer blend composed of salmon gelatin (SG), chitosan (Ch), and poly(vinyl alcohol) (PVA) was developed by electrospinning onto a micropatterned (MP) collector, resulting in a biomimetic scaffold for seeding muscle cells. Rheology and surface tension studies were performed to determine the optimum solution concentration and viscosity for electrospinning. The scaffold microstructure was analyzed using SEM to determine the nanofiber's diameter and orientation. Blends of SG/Ch/PVA exhibited better electrospinnability and handling properties than pure PVA. The resulting scaffolds consist of a porous surface (∼46%), composed of a random fiber distribution, for a flat collector and scaffolds with regions of aligned nanofibers for the MP collector. The nanofiber diameters are 141 ± 2 and 151 ± 2 nm for the flat and MP collector, respectively. In vitro studies showed that myoblasts cultured on scaffold SG/Ch/PVA presented a high rate of cell growth. Furthermore, the aligned nanofibers on the SG/Ch/PVA scaffold provide a suitable platform for myoblast alignment.

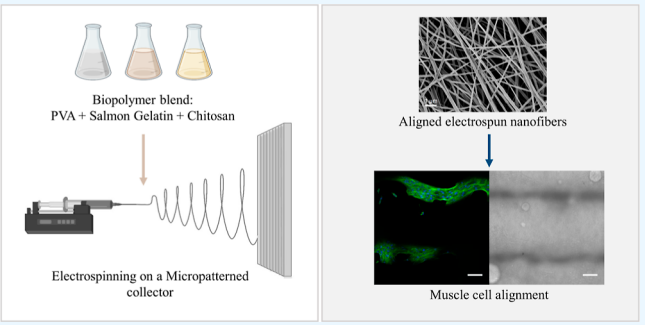

1. INTRODUCTION

A requirement in skeletal muscle tissue engineering (SMTE) is the development of scaffolds that facilitate cell alignment in aims of directing skeletal muscle regeneration and growth.[1] To achieve this, scaffolds should mimic the hierarchical structures found in the extracellular matrix (ECM) of the native muscle tissue.[2] The ECM is a complex natural viscoelastic scaffold,[3] composed of a dense and functional protein assembly that includes nonfibrillar collagen type IV, laminin, fibrillar collagen type I, proteoglycans, and sulfated glycosaminoglycans,[4,5] with a unique tissue-specific architecture.[6] This matrix provides a three-dimensional structure and a microenvironment for cells to modulate different biological processes, such as cell attachment, migration, proliferation, differentiation, cell−cell signaling, and ECM deposition.[7]

Skeletal muscle tissue has a highly organized structure, composed of parallel elements that can be divided into fascicles, myofibers, and myofibrils.[1,8] In this context, the distinctive well-structured layout of the native ECM has been described as one of the most critical factors in skeletal regeneration, by facilitating the longitudinal migration and proliferation of satellite cells.[1,2,9]

Several tissue engineering strategies have been used to manufacture scaffolds that mimic the ECM and its topography. Fernández-Costa et al.[10] suggested that these approaches can be classified into three main types: micropatterning, e.g., photolithography and soft lithography,[11] electrospinning, and bioprinting.

Micropatterning has been extensively used to create unidirectional patterns over the surface of polymers to promote the prealignment of muscle cells. In a previous work, we reported an edible biopolymer film of alginate and fish gelatin, shaped using a micropattern mold with parallel microchannels (∼70 μm). The designed surface showed to be biocompatible and suitable for laying muscle cells in a fiber-like array.[12] Recently, Denes et al. reported that growing C2C12 myotubes on micropatterned (MP) gelatin hydrogels accelerates sarcomere formation relative to myotubes cultured on unpatterned gelatin and plastic.[13] Additionally, Denes et al. found an upregulation in genes related to sarcomere formation and in vivo muscle maturation in the myotubes associated to growth on MP gelatin hydrogels. Other authors have also established that micropatterning technologies can be used to

Received: August 28, 2023
Revised: November 16, 2023
Accepted: November 17, 2023
Published: December 5, 2023

control skeletal muscle differentiation and tissue architecture.[14−16]

However, considering the fibrous elements of the ECM, it is relevant to develop aligned nanofiber scaffolds with anisotropic structures that resemble the ECM of skeletal muscle. Among various techniques found in the literature, e.g., electrospinning, molecular self-assembly, and thermally induced phase separation, electrospinning has become a relevant and straightforward approach to produce nanofibers for scaffolds.[11] Electrospinning has been widely used due to the similarity between electrospun nanofibers and the collagen fibrils found in the native ECM (10−500 nm in diameter).[11,17] This similarity can be used in biomedical and tissue engineering applications.[18,19] Normally, electrospun fibers are collected on flat two-dimensional plates. These flat collectors give way to randomly arranged fibrous membranes,[20] affecting the distribution, morphology, and biological function of the seeded cells.[21,22] Other experimental approaches have been made to produce aligned fibrous-like elements within scaffolding materials. For example, using a high-speed rotating drum collector or modifying the geometry of the grounded target.[23] MP collector-based electrospinning[24] combines the basic principle of the electrospinning process using a custom-made patterned conductive collector instead of a flat-grounded target.[25]

On the other hand, synthetic and natural biocompatible polymers, or a combination of both, including poly(lactide-*co*-glycolide) (PLGA),[26] polyurethane (PU),[27] polycaprolactone (PCL),[28] collagen,[29,30] fibrin,[31] silk fibroin,[32] PCL−collagen,[9] chitosan (Ch)−PCL,[33] Ch−poly(vinyl alcohol) (PVA),[34] and polyhydroxyalkanoate,[35] have been used to fabricate electrospun nanofiber scaffolds for SMTE. Recently, Ligouri et al.[36] published the use and characterization of cross-linked electrospun fish gelatin mats, although further studies are necessary to probe if it is suitable for biomedical applications. In previous studies, we have demonstrated the use of salmon gelatin (SG) to fabricate scaffolds for biomedical applications using different approaches, e.g., cold casting[12] and freeze-drying.[37−39]

Gelatin is a fibrillar protein produced by denaturation and partial hydrolysis of collagen which is the main constituent of the ECM.[40] Among the advantages of using fish gelatin in SMTE applications are its inherent biological recognition properties [arginine, glycine, and aspartic acid (RGD) motif], which promote cell adhesion and migration.[41] Besides, fish gelatin is biocompatible,[37] readily available, and has little or no possibility of zoonosis.[42,43] Ch is a natural polymer derived from the partial deacetylation of chitin from crustacean shells, that has a structure analogous to glycosaminoglycans.[44] Furthermore, it has been reported that Ch forms a polyelectrolyte complex with gelatin, enhancing its physical, mechanical, and biological properties.[45]

However, to produce nanofibers from SG and Ch blends, a common approach is to incorporate these polymers within a polymer matrix, such as PVA or poly(ethylene oxide) (PEO).[40,46,47] PVA is a semicrystalline, water-soluble polymer produced on an industrial scale by partial hydrolysis of poly(vinyl acetate) (PVAc).[48] PVA has good mechanical properties, is biocompatible, and nontoxic[49] with various biomedical applications, such as drug delivery systems, wound dressing, artificial skin, and cardiovascular devices.[50,51]

In this research, MP nanofiber scaffolds were prepared using different ratios of SG, Ch, and PVA. The SG/Ch/PVA nanofiber scaffolds were fabricated using a custom-made MP collector plate to control the spatial arrangement of electrospun fibers during the electrospinning process. The aligned topographical features in the MP collector were designed and manufactured with a computer numerical control (CNC) milling machine. Finally, C2C12 cells were seeded on the MP electrospun scaffolds, and viability, distribution, morphology, and cell behavior were investigated over the scaffolds up to 72 h.

To our knowledge, there is no other study published on MP electrospun scaffolds using a mixture of SG/Ch/PVA for SMTE applications. The cell behavior and growth of the C2C12 cells were enhanced and orientated because of the topographical features of the SG/Ch/PVA scaffolds.

2. MATERIALS AND METHODS

2.1. Materials. PVA (MW 89,000−98,000, 99+% hydrolyzed) to fabricate the electrospun polymer matrix was purchased from Sigma-Aldrich Inc. (St. Louis, MO, USA). SG from Atlantic salmon skins (*Salmo salar*) was extracted and provided by Enrione et al.[39] and has been used in a previous study by Acevedo et al.[38] to fabricate bioactive scaffolds. Ch (pharmaceutical grade, 95% deacetylated, 300 kDa, derived from crab shells) was purchased from Quitoquimica (Concepción, Chile).

EDC 1-ethyl-3-[3-(dimethylamino)propyl)] carbodiimide hydrochloride, NHS (*N*-hydroxysuccinimide 98%), MES [2-(*N*-morpholino) ethanesulfonic acid], ethanol (EtOH) (p.a., 99.8%), acetic acid (CH_3COOH), and other chemicals of reagent grade were purchased from Sigma-Aldrich Inc. (St. Louis, MO, USA).

CellTiter-Glo luminescent cell viability assays were purchased from Promega (Madison, WI, USA). The fluorescent probes Rhodamine Phalloidin R415 and SYTOX Green nucleic acid stain; Dulbecco's modified Eagle's medium (DMEM) high glucose, no glutamine; fetal bovine serum (FBS), penicillin, streptomycin, L-Glutamine, phosphate-buffered saline (PBS), 0.25% trypsin ethylenediaminetetraacetic acid (Trypsin-EDTA), and trypan blue dye were all purchased from Thermo Fisher Scientific (Massachusetts, USA).

To prepare the solutions and washing procedures, water (>18.2 MΩ cm) from a PURELAB classic ELGA Milli-Q system (Paris, France) was used.

2.2. MP Collector Plate Design and Fabrication. MP collector plates were designed in Autodesk Fusion 360 software (version 2019, Autodesk, Inc. Mill Valley, CA, USA) and manufactured with a CNC milling machine (Datron M8, Datron AG, Germany), using Duralumin as a substrate; 10 cm × 10 cm squared structures with a thickness of 10 mm were cut. The grooves were made by using a 90° angle tapered end mill. The advance speed was 400 mm/min, and the rotation speed was 10,000 rpm in conjunction with the use of cooling liquid to avoid deformations in the termination of the grooves. The morphology and microstructure of the MP collector plate were characterized using a stereoscopic microscope (Nikon, model SMZ800N, Tokyo, Japan).

2.3. Electrospinning Solution Preparation. Electrospinning solutions were prepared as follows. Commercially available PVA (20% w/w) and SG (3% w/v) were dissolved separately under gentle stirring in Milli-Q water at 90 °C for 5 h and 50 °C for 3 h, respectively. Ch (3% w/v) was dissolved in Milli-Q water with acetic acid (0.5 M) at 60 °C for 3 h until

https://doi.org/10.1021/acsomega.3c06436
ACS Omega 2023, 8, 47883−47896

a clear and homogeneous solution was obtained, followed by a gentle centrifugation to remove air bubbles.

The PVA and SG/Ch/PVA blend solutions were prepared according to the ratios shown in Table 1 and stirred for 1 h at 70 °C with constant stirring at 300 rpm. To facilitate the electrospinning process, PVA was added to each solution, except for sample M8.

Table 1. Spinning Solutions of SG/Ch/PVA

sample ID	SG/Ch/PVA ratio	SG concentration (w/v %)	Ch concentration (w/v %)	PVA concentration (w/w %)
M1	0:0:100	0	0	10
M2	50:0:50	1.5	0	10
M3	40:10:50	1.2	0.3	10
M4	30:20:50	0.9	0.6	10
M5	20:30:50	0.6	0.9	10
M6	10:40:50	0.3	1.2	10
M7	0:50:50	0	1.5	10
M8	50:50:0	1.5	1.5	0

2.4. Electrospinning. The electrospinning setup consists of a homemade acrylic chamber and a Teflon rail (Figure S1). The Teflon rail was used to align and control the distance between the syringe needle and collector. The syringe needle and collector plate were held onto the rail by homemade Teflon holders. The collector is a homemade steel plate (flat collector) which can be used to glue a MP collector. The syringe needle (Ramé-hart Instrument Co., Washington, USA) was connected to a 50 kV high-voltage power supply device (Tong Li Tech, Shenzhen, China). The polymer solution was placed within a syringe (Nipro, Osaka, Japan) outside of the acrylic chamber and fed through the needle by a syringe pump driver system (New Era Pump Systems, Inc., NY, USA). Details of this setup are depicted in Supporting Information Figure S1.

Spinning solutions of SG/Ch/PVA (Table 1) were loaded into a 10 mL syringe with a 19 Gauge stainless steel needle. A syringe pump was used to control the solution outflow at a constant flow rate of 0.20 mL/h.

The electrospun nanofiber scaffolds were fabricated by applying a 7 kV potential between the solution and the grounded collector plate. The spinning distance was 10 cm, and the exposure time (ET) was 4 h per solution. The experiments were performed at room temperature, and relative humidity was constantly monitored. The resulting electrospun nanofiber scaffolds were peeled off from the collector plate (MP or flat) and stored in Petri dishes that were then placed in a plastic container with silica gel beads.

2.5. Rheological Properties. The shear viscosities were measured by using a two-plate rheometer (Discovery Hybrid HR-3; TA Instruments, New Castle, DE, USA). The DHR-3 is equipped with an Advanced Peltier Plate 40 mm, a solvent trap filled with distilled water, and an evaporation blocker. The gap size between plates was 1 ± 0.2 mm. The amplitude sweeps were carried out at 25 °C. The shear rate range (γ) was between 0.01 and 1000 s^{-1}.

2.6. Surface Tension. The surface tension (γ) of the SG/Ch/PVA solutions was measured at room temperature by the Du Noüy ring method using a DCAT 21 tensiometer (DataPhysics Instruments). Fresh Milli-Q water was used as the experimental reference.

2.7. Fourier Transform Infrared Spectroscopy Characterization. Attenuated total reflectance Fourier transform infrared spectrophotometry (ATR-FTIR, Bruker Tensor II with Platinum ATR-Unit, Germany) was used to characterize the absorption peaks of the SG/Ch/PVA electrospun nanofibrous scaffolds. SG/Ch/PVA electrospun scaffolds were cut into small pieces (10 × 10 mm) and FTIR spectra were obtained in the mid-infrared region of 4000−500 cm^{-1}, by averaging 32 scans with a resolution of 4 cm^{-1} at room temperature. The obtained spectra were baseline-corrected, and then the major vibration bands were associated with the main chemical groups of SG, Ch, and PVA on the polymer blends.

2.8. SEM Nanofiber Scaffold Characterization. The morphology of the SG/Ch/PVA nanofiber scaffolds was analyzed by scanning electron microscopy (SEM, Zeiss, LEO 1530 Gemini, Jena, Germany) using a voltage of 3 kV, coupled to an aperture of 30 μm and a working distance of 4.9 mm. Prior to the analysis, the scaffolds were cut (5 × 5 mm^2) and sputter coated with a thin layer of platinum (7 nm).

To determine the diameter distribution and fiber orientations of the SG/Ch/PVA nanofiber scaffolds, the SEM images were analyzed with ImageJ Software (NIH, version 1.50i, Bethesda, MD, USA) with the DiameterJ and OrientationJ plugins, as described in previous studies.[52,53] The average fiber diameters are shown as histogram distributions. The relative mean fiber orientations were presented as polar plots over a +90/−90° range.

2.9. Cross-Linking of SG/Ch/PVA Nanofibrous Scaffolds. Prior to in vitro analysis, the SG/Ch/PVA electrospun scaffolds were cut into small pieces (10 × 10 mm), sterilized (EtOH 70% v/v for 2 h), and soaked in a cross-linking bath with a solution of EDC (30 mM) and NHS (8 mM), using MES (50 mM) as buffer and EtOH (90% v/v) as solvent at room temperature for 2 h. The resultant cross-linked scaffolds were washed three times with EtOH (70% v/v) and Milli-Q water to remove residual solvents introduced during the electrospinning and cross-linking process.

2.10. Cell Culture. The mouse (*Mus musculus*) myoblast cell line C2C12 (ACC 565) was purchased from the German Collection of Microorganisms and Cell Cultures (DSMZ, Braunschweig, Germany). C2C12 cells were cultured based on standard protocols for cell culture.[12] Myoblasts were used between passages 5−14 and maintained in DMEM high glucose supplemented with 10% of FBS, 1% of L-glutamine (2 mM), and 1% of antibiotics (100 U/ml penicillin and 100 μg/mL streptomycin) at 37 °C in a humidified atmosphere with 5% CO_2 and 95% air. The medium was changed twice a week, and the cells were subcultured before reaching confluence every 3−4 days.

2.11. Cell Culture over SG/Ch/PVA Nanofibrous Scaffolds. The cross-linked SG/Ch/PVA nanofiber scaffolds were transferred into a 96-well Flat Bottom Polystyrene plates (Greiner Bio-One, Kremsmünster, Austria) and conditioned with 200 μL of DMEM high glucose supplemented (10% of FBS, 1% of L-glutamine, and 1% of antibiotics) at 37 °C and 5% CO_2 for 24 h. After conditioning, the medium was removed from the wells. Then, the C2C12 cells were trypsinized (0.25% Trypsin-EDTA) and counted with an automated cell-counter TC10 (BioRad; California, USA) using trypan blue dye. Subsequently, myoblasts were cultured over the conditioned SG/Ch/PVA nanofiber scaffolds at a seeding density of 3 × 10^3 cells/well in 100 μL of DMEM high glucose supplemented

https://doi.org/10.1021/acsomega.3c06436
ACS Omega 2023, 8, 47883−47896

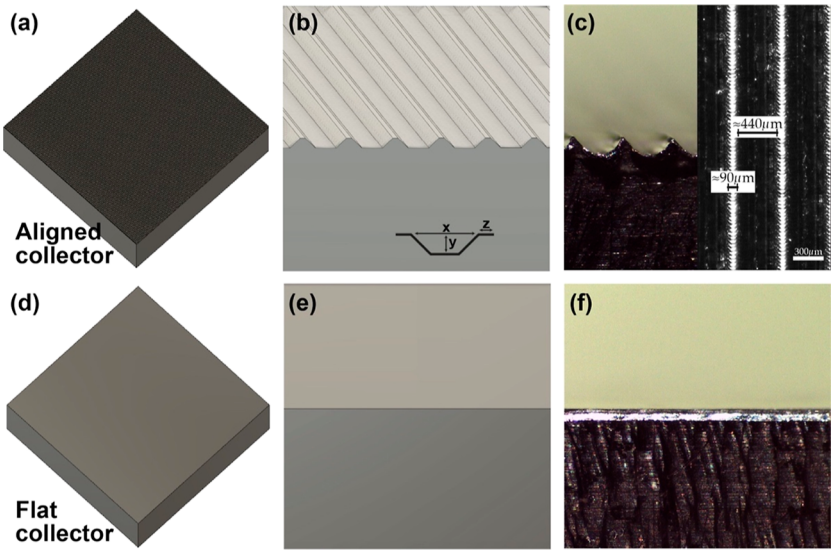

Figure 1. Schematic representation of the collector plates, design, and manufacture. (a,b) Representative figure of the MP collector plate; (c) sideview micrograph of the aligned collector, *x*: channel width ≈440 μm; *y*: channel height ≈160 μm; *z*: ridge width ≈90 μm; (d,e) representative figure of the flat (control) collector plate used in the electrospinning process; and (f) sideview micrograph of the flat collector plate.

with 10% of FBS, 1% of L-glutamine, and 1% of antibiotics. Cells cultured over the flat white polystyrene wells (FPW) without the nanofiber scaffolds, with DMEM high glucose supplemented with 10% of FBS, 1% of L-glutamine, and 1% of antibiotics and with or without DMSO 20% (w/w), were used as positive and negative controls, respectively. The C2C12 cells were incubated in a humidified atmosphere of 5% CO_2 at 37 °C for 4, 24, 48, and 72 h before performing the cell viability assay.

2.12. Cell Viability Assay. In vitro studies were used to determine the viability and cellular behavior of C2C12 cells when cultured and exposed to SG/Ch/PVA nanofiber scaffolds during 4, 24, 48, and 72 h. The viability and cellular behavior of C2C12 cells were evaluated by the CellTiter-Glo luminescent cell viability assay. This method is based on the quantitation of the ATP present, which indicates the metabolically active cells in culture. CellTiter-Glo reagent was prepared and used according to the manufacturer's instructions.

At the end of each incubation period (4, 24, 48, and 72 h), 100 μL of CellTiter-Glo was added to each well followed by a mixing step with an orbital shaking for 2 min to induce cell lysis and an incubation step at room temperature in the dark for 10 min. Luminescence was recorded by using an Infinite M1000 plate reader (Tecan, Männedorf, Switzerland). All the viability experiments were carried out in triplicate and compared to the appropriate controls (positive control, C2C12 cells in DMEM with DMSO 20% and negative control, only C2C12 cells in DMEM). The data from the experiments were expressed as percentage for the viability and as luminescence in relative light units (RLU) for the cellular behavior assays, both termed control conditions. Results are expressed as mean of the triplicate ± standard deviation.

2.13. Immunocytochemistry by Laser Scanning Confocal Microscopy. The morphology and distribution of C2C12 cells on the SG/Ch/PVA nanofiber scaffolds were determined by fluorescent staining techniques with SYTOX Green nucleic acid stain and Rhodamine Phalloidin R415, applied according to the manufacturer's instructions. MP and Flat nanofiber scaffolds were cut (10 × 10 mm), cross-linked, and conditioned as previously described. Myoblasts were seeded at a density of 2.6×10^5 cells/cm^2 on Ibidi plates μ-Slide 8 Well (Ibidi, Martinsried, Germany) and incubated for 72 h in a humidified atmosphere of 5% CO_2 at 37 °C.

After incubation, myoblasts cultured onto the nanofiber scaffolds were gently washed twice with PBS and fixed with 4% of p-formaldehyde in PBS at room temperature for 10 min, followed by three washing steps with TBS. Then, C2C12 cells were permeabilized with 0.1% of Triton X-100 in TBS for 5 min, then washed two times with TBS. Actin filaments and nuclei were simultaneously stained for 30 min at room temperature with Rhodamine Phalloidin R415 (1×) and SYTOX Green (1×), respectively. Images were acquired using a laser scanning confocal microscope LSM SP5 STED (Leica Microsystems, Wetzlar, Germany) with an HC PL APO CS2 20*x*/0.75 IMM water immersion objective lens. The maximum excitation and emission wavelengths were chosen according to the dyes used. To monitor SYTOX, a 488 nm excitation argon laser was used and detected at 500−547 nm. Rhodamine Phalloidin was excited by a 488 nm argon laser and detected at 597−737 nm. The laser scanning confocal microscopy (LSCM) images were analyzed by using ImageJ software and Leica Application Suite X (Version 4.1.1, Leica Microsystems, Wetzlar, Germany).

2.14. Statistical Analysis. All statistical analyses were performed using Excel (version 16.62 Microsoft) and OriginPro (Version 2022b OriginLab Corporation). All variables were tested in three independent cultures for each experiment, which was repeated twice ($n = 6$). All results were expressed as the mean ± standard deviation. Statistical comparisons were carried out by a two-way analysis of variance (ANOVA), and a Tukey's post hoc test was performed for multiple comparisons in the viability assays. When indicated, a value of $p < 0.05$ was considered statistically significant.

3. RESULTS AND DISCUSSION

3.1. Collector Plate Manufacture. To obtain SG/Ch/PVA scaffolds with uniaxially aligned nanofibers, we designed the MP collector plate with parallel microchannels, as shown in

https://doi.org/10.1021/acsomega.3c06436
ACS Omega 2023, 8, 47883−47896

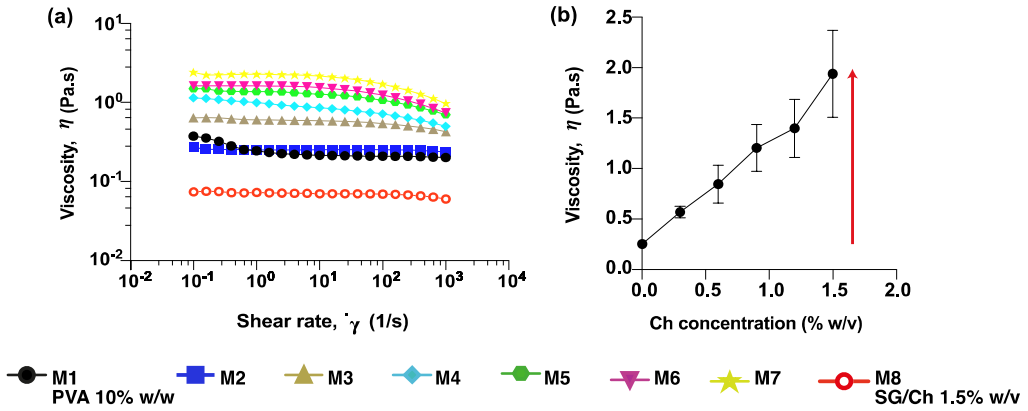

Figure 2. Flow curve. (a) Shear viscosity as a function of shear rate for PVA and SG/Ch/PVA polymer solutions; (b) shear viscosity as a function of Ch concentration. Solutions were prepared as shown in Table 1.

Figure 1. The depth of the grooves (y) was around 160 μm, and their width (x) was 440 μm. The repetition length of the micropattern was approximately 530 μm. The ridge width (z) was 10% smaller than the original CAD design.

Considering that muscle fibers size range between 20 and 100 μm[1], the size and shape of the designed channels in the collector plate are within the diameter range to produce MP nanofiber scaffolds of SG/Ch/PVA.

3.2. Solution Properties. Physical and chemical parameters such as solution viscosity, surface tension, electric conductivity, and polymer concentration are critical factors during the electrospinning process, that are known to affect the spinnability, morphology, and size of electrospun nanofibers.[17] Ch is a polymer that has poor solubility and a high viscosity in aqueous solution.[54] Conversely, fish gelatin is a water-soluble polymer with low rheological properties.[55] Since gelatin and Ch can interact and form a polyelectrolyte complex, various ratios of SG/Ch blends might exhibit different rheological characteristics. PVA was added to increase the spinnability of the solution and influence the morphology of the nanofibers.

Therefore, to analyze the flow behavior of SG/Ch/PVA blend solutions and how the variation of Ch content in the solution affects the viscosity and, consequently, the spinnability of the solutions (Table 1), shear viscosity as a function of shear rate was measured for all solutions. Results of this analysis are shown in Figure 2. As expected, the viscosity of the solutions was found to increase with increasing Ch content in the SG/Ch/PVA blends (Figure 2a). This change in viscosity is not related to the SG content in the mixture due to its low rheological properties when compared to mammalian gelatin. However, it has been reported that Ch alters the helical structure of collagen by forming ionic bonds and a hydrogen-bonding network, which increased the viscosity of the blend,[56] as shown in Figure 2b. Similar results have been reviewed with fish gelatin by Gómez-Guillén et al.[57]

The viscosity of polymer solutions can exhibit three main mechanical responses as a function of the shear rate: Newtonian, shear thinning, and shear thickening. We observe that once Ch is added, blends M3 to M7 underwent a shear-thinning process with increasing shear rates (Figure 2a). Shear thinning in samples M3−M7 decreases with Ch content and is lowest for the solution with the lower amount of Ch (M3). The dependence on the shear rate is close to Newtonian for solutions without Ch (M1 and M2 blends).

Adding Ch improved the rheological properties of the blend and considerably increased the viscosity of the solutions, as illustrated in Figure 2a. The blends with PVA and increasing Ch content (M2 to M7) have a much higher viscosity (0.25223 ± 0.00595 to 1.93943 ± 0.43017 Pa·s) in comparison with the M8 blend (0.07013 ± 0.00352 Pa·s). Moreover, both SG and Ch can interact with PVA through hydrogen bonding between the polar groups of the fish gelatin and hydroxyl moieties of Ch and PVA in the blends, thus facilitating the electrospinning process.[58]

3.3. Surface Tension. During the electrospinning process, when sufficient voltage is applied, the polymer solution forms a cone at the end of the tip, known as the Taylor cone. Once the electrostatic forces overcome the surface tension of the polymer solution, the formation of fibers toward the collector plate is initiated.[59,60] To search for polymer solutions suitable for electrospinning, the viscosity and surface tension of SG/Ch/PVA blend solutions were determined, as shown in Table 2.

Table 2. Viscosity and Surface Tension of GS/Ch/PVA Solutions

	sample ID	viscosity η (Pa·s)	surface tension (mN/m)
Milli-Q water	M0		71.698 ± 0.061
PVA	M1	0.2396 ± 0.05128	66.142 ± 0.152
SG/PVA	M2	0.25223 ± 0.00595	62.312 ± 0.096
SG/Ch/PVA	M3	0.56937 ± 0.05935	61.345 ± 0.285
	M4	0.84761 ± 0.18878	64.531 ± 0.332
	M5	1.20493 ± 0.23162	60.454 ± 0.442
	M6	1.39798 ± 0.28912	63.772 ± 0.447
Ch/PVA	M7	1.93943 ± 0.43017	64.446 ± 0.351
SG/Ch	M8	0.07013 ± 0.00352	57.007 ± 0.070

Table 2 shows the differences between the viscosity ($P < 0.01$) and the surface tensions ($P < 0.01$) of the samples. Surface tension values were all lower than Milli-Q water (71.698 mN/m)[61] and pure PVA 10% w/w (66.142 mN/m). The values reported for the surface tension of PVA at different molecular weights and concentrations can range from 38.46[62] to 72 mN/m[63] for PVA_{88000} and PVA_{125000}, respectively.[62] According to Rošic et al.,[63] with an increasing concentration of PVA, the surface tension will also increase and reach similar values as the surface tension of pure water (72 mN/m) at concentrations higher than 10% w/w. Similar values (66.142

https://doi.org/10.1021/acsomega.3c06436
ACS Omega 2023, 8, 47883−47896

mN/m) were obtained during our measurements for PVA_{98000} 10% w/w.

Furthermore, as expected, the addition of PVA to the SG/Ch blends increased the surface tension of the solutions (M2 to M7), since the surface tension of PVA (66.142 ± 0.152 mN/m) is lower than the pure water (71.698 ± 0.061 mN/m) but higher than the M8 solution. Furthermore, the presence of −OH groups in PVA has been reported to increase H bonding with Ch molecules and other organic polymers, improving the electrospinnability of the solutions.[58] This was further verified by FTIR analyses. Additionally, for the samples with increasing concentrations of Ch (M3, M4, M5, and M6), the mean values of surface tension varied between 60−64 mN/m, which can be also attributed to the low surface tension of pure acetic acid (27.08 mN/m).[64] At the Ch concentrations shown in Table 2, the electrical and rheological properties of the polymer solution are more stable. According to the SEM micrographs, M4 solutions exhibit better spinnability, which significantly affects the production of nanofibers. This will be further discussed in the SEM analysis (Section 3.5).

3.4. FTIR Analysis. FTIR spectroscopy was done on 10 × 10 mm^2 pieces of the SG/Ch/PVA electrospun scaffolds. FTIR analyses were performed prior to cross-linking for biological assays, to assess the presence of the blended components (CH and SG) within the PVA matrix. Not all solutions were successfully electrospun (M6−M8). The M7 and M8 solutions were especially difficult to electrospin, with a nonstable formation of the Taylor cone and an uneven deposition (for M7 solution) or nonpolymer deposition on the collector plate (for M8 solution). This decrease in the electrospinning efficiency is probably due to the increased Ch concentration of the blend, evidenced by the high viscosity of the solution M7 (1.93943 ± 0.43017 Pa·s) vs M8 (0.07013 ± 0.00352 Pa·s), or the absence of the PVA in the blend (M8 solution). Furthermore, some of the obtained scaffolds (M2, M3, M5, M6, and M7) were too brittle to handle, or did not produce a scaffold, i.e., there was not enough available material for biological cell behavior assays (Figure S2). However, there is still enough material for FTIR measurements.

FTIR spectra of PVA (M1) and SG/Ch/PVA scaffold blends (M2, M3, M4, and M5) are summarized in Figure 3. M1 spectra show the characteristic functional groups of pure PVA. The large peak at 3296.4 cm^{-1} corresponds to the nonbonded OH stretching vibration band (hydroxyl groups for free alcohol).[65] The following duplet absorption peaks at about 2940.3 and 2911.7 cm^{-1} are linked to the C−H alkyl stretching band related to aldehydes.[66] The remaining large band at 1422.9 cm^{-1} corresponds to acetate groups (C−O), due to the saponification reaction of polyvinyl acetate.[67] The band intensity at 1089.7 cm^{-1}, according to Mansur et al.,[66] is related to the crystalline portion from the PVA degree of hydrolysis (DH), which in this case is 99%.

The overall spectra of the blended samples come mostly from the PVA. The characteristic frequencies of amide groups from SG and Ch tend to overlap those of hydroxyl and acetate groups of PVA. As reported in the Supporting Information (Table S1), all the scaffold blends except for the pure PVA electrospun scaffold showed the typical amide I, II, and III bands, which are characteristic of fish gelatin and Ch.[68−71]

The FTIR spectrum presented broadbands in the frequency at around 3300−2911 cm^{-1} in all the SG/Ch/PVA blends, attributed to water-mediated hydrogen bonding from both hydroxyls (−OH, Ch and PVA) and amino (N−H, SG/Ch)

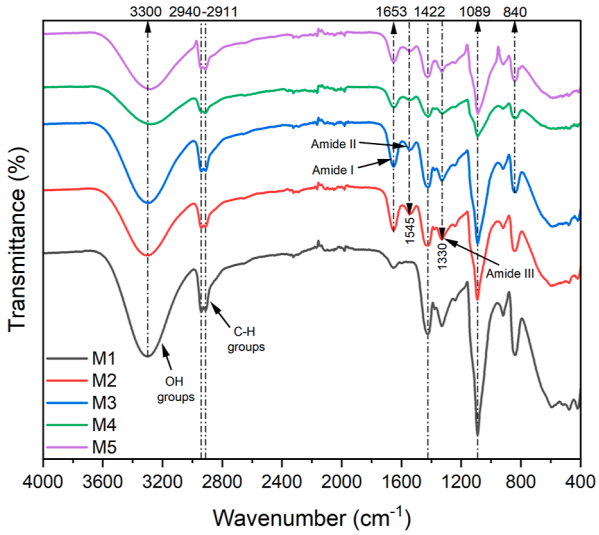

Figure 3. FTIR spectra from SG/Ch/PVA electrospun nanofiber scaffold blends.

symmetrical vibration interactions.[70,71] However, the absorption bands at 3300 cm^{-1}, decrease in intensity and shift slightly toward lower numbers by 7.15, 21.45, and 4.29 cm^{-1}, for M3, M4, and M5, respectively. Furthermore, comparing the spectra of M1 with the blends M2 to M5, we observe changes in the main absorption band intensities related to SG (amide I, amide II, and amide III bands between 1653 and 1330 cm^{-1}) and Ch blends (saccharide bands 1100−840 cm^{-1}). The characteristic absorption peak of fish gelatin, C═O and N−H bending vibrations in amide I region,[71] shifts to lower wavenumbers, from 1653.2 to 1648.9 cm^{-1} (from M2 to M5), with decreasing SG blending ratio. Staroszczyk et al.[71] reported that the reduction in the amide I region is due to the interaction of fish gelatin and Ch by the formation of a helical structure (single α-helix). In Figure 3 (M3, M4, and M5), between 1540 and 1330 cm^{-1}, the other amide bands of SG (amide II and III) decreased in intensity. Amide II bands appeared in the spectrum between 1545 and 1372 cm^{-1} once SG is present in the blend. This peak can be attributed to the formation of hydrogen bonds in which N−H bending vibrations are coupled to C−N stretching vibrations of this protein.[69−71] The FTIR spectra for samples M2−M5 showed a slight shift (2.8 cm^{-1}) and a change in the intensity between 1422.9−1420.1 cm^{-1}, relative to the ratio of SG and Ch in the blend, corresponding to the symmetric −COO−, $-CH_2$ and $-CH_3$ groups of gelatin and Ch.[68] The shift to lower wavenumbers, considering SG content, was attributed to −COO− vibrations.[71] Meanwhile, the decrease in the amide II band with Ch blending ratio indicates the presence of carboxylic acid in the polymer blend. This was attributed to the acetic acid used for dissolving the Ch in this study.[70,72,73] We also noticed that the characteristic peak at around 1700 cm^{-1}, corresponding to carboxylic acid, was not identified, which suggests that there was no free acetic acid in all the blends tested. This confirms that the amino groups of Ch became protonated, allowing the formation of electrostatic interactions involving the NH_3^+ groups of Ch and the −COO− groups of the aspartic and glutamic residues in collagen.[70] Amide III peaks at about 1330 cm^{-1} were assigned to the C−N and N−H vibrations characteristic of SG and Ch.[71]

https://doi.org/10.1021/acsomega.3c06436
ACS Omega 2023, 8, 47883−47896

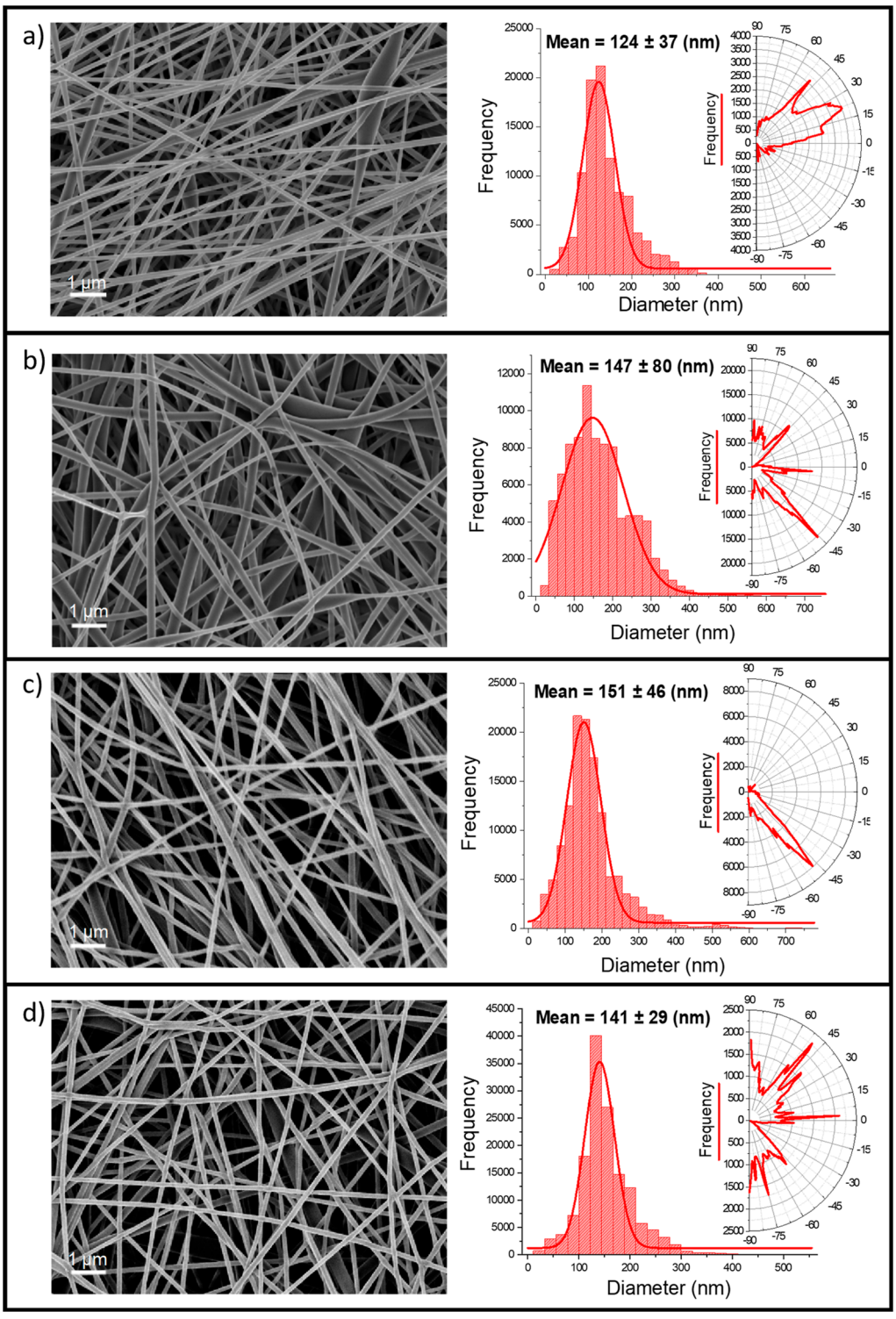

Figure 4. SEM micrographs of the PVA and SG/Ch/PVA nanofiber scaffolds. Each micrograph with respective fiber diameter and orientation distribution. (a) M1-MP; (b) M1-Flat; (c) M4-MP; and (d) M4-Flat.

In Figure 3, the samples blended with Ch (M3, M4, and M5) presented the characteristic absorption bands of Ch between 1088.3 and 836.6 cm^{-1}, corresponding to the saccharide structure.[70,73] The shift by 4.2 cm^{-1} toward higher wavenumbers and the change in the band intensity at around 840 cm^{-1} for M3, M4, and M5 are due to the influence of the hydroxyl and ether oxide bands of Ch[71,73] and the decreasing intensity of amide bands of SG, respectively. Similar findings were reported by Staroszczyk et al. for fish gelatin from Baltic cod (*Gadus morhua*) skins.[71]

The tested blends of SG/Ch/PVA had significant differences among samples, suggesting that FTIR analysis is highly sensitive to small ratio changes in SG and Ch. All the previous observations, accompanied by the appearance of new peaks, clearly indicate the existence of good miscibility between SG, Ch, and PVA and the formation of a three-component scaffold.

https://doi.org/10.1021/acsomega.3c06436
ACS Omega 2023, 8, 47883−47896

This has been extensively reported for two-component blends: collagen/Ch;[73] PVA/Ch;[74] and PVA/collagen.[49] There have been fewer reports on ternary blends of gelatin, Ch, and PVA found in the literature.[75]

3.5. Nanofiber Scaffold Morphology. Many parameters, such as viscosity, surface tension, and electrospinning parameters (applied voltage, flow rate, and working distance), influence the morphology and diameter of electrospun nanofibers. PVA and SG/Ch/PVA nanofiber scaffolds were produced by electrospinning and characterized by SEM. Figure 4a−d, shows the nanofiber morphology, diameter, and orientation distribution for PVA and SG/Ch/PVA nanofiber scaffolds. Samples (M1 and M4) were selected according to the handling properties and manipulation of the fabricated scaffolds (Figure S2). SEM images of samples M1 and M4 (Figure 4a−d) show that the nanofiber scaffolds were porous, as seen for all of the analyzed samples. Scaffolds were grouped according to the employed collector plate, i.e., flat or MP. The presence of beading was dependent on the formulation used during the electrospinning process.

Figure 4a,b presents the resulting nanofiber scaffolds of formulation M1 (PVA 10 w/w %) MP and Flat, with a mean fiber diameter of 124 ± 37 and 147 ± 80 nm. Park et al.[76] previously reported fiber diameters for PVA 8−12 wt % (190, 200, 220, and 470 nm, with a DH of 88, 92, 96, and 99.9%, respectively) and suggested that the fiber diameter increased exponentially with respect to the DH of the PVA. However, the MW of the PVA or the porosity of the fabricated scaffolds were not reported.

SEM images show that the nanofiber scaffold M1 had a porous structure (Figure 4a,b) and interconnected pores. The SEM obtained porosity of the scaffold's surface ranges between 40 and 43% porosity (Table 3). However, the percentage surface porosity values of pure PVA nanofiber scaffolds were slightly smaller than those of SG/Ch/PVA nanofiber scaffolds, which can be attributed to the viscosity of the pure PVA and the presence of bead-like defects on M1 nanofiber scaffolds (further discussed in this section), so the pore % became small (around 6% just for the MP scaffolds).

Table 3. Mean Fiber Diameter and Surface Porosity of PVA and SG/Ch/PVA Nanofiber Scaffolds

sample ID	mean fiber diameter [nm]	surface porosity [%]
M1-MP	124 ± 37	40
M1-Flat	147 ± 80	43
M2-MP	105 ± 32	44
M2-Flat	116 ± 35	57
M3-MP	125 ± 62	50
M3-Flat	116 ± 50	52
M4-MP	151 ± 46	47
M4-Flat	141 ± 29	46
M5-MP	405 ± 67	47
M5-Flat	450 ± 120	42

The micrograph in Figure 4a,b shows a mat formation composed of a complex web of fibers and a few bead-like defects on the surface and in between the layers of the scaffold. High MW PVA was used to produce nanofiber scaffolds from 10% (w/w) solutions. According to Rwei and Huang,[62] this concentration is in the range that yields an acceptable electrospinning process. Furthermore, Zhang et al.,[77] reported that the DH value of PVA should not be less than 88% to achieve a good electrospinning process.[77] Nevertheless, the surface tension is still the main driver when it comes to bead formation during the electrospinning process, regardless of whether the failure is associated with an excessively diluted or concentrated spinning solution.[62]

On the other hand, the polar plot in Figure 4a demonstrated that the fibers of the sample M1-MP were more aligned in comparison to the flat collector, with a relative mean fiber orientation ranging between 9 and 49°. Although there is a spread in the orientation of the aligned fibers, a preferred fiber direction was observed at 22°. The nanofiber scaffold presented in Figure 4b has a random distribution with no dominant fiber orientation, expressed with a relative mean fiber orientation ranging between 46 and −46°. This complete randomness is due to an unstable and whipping motion of the electrospinning jet, generally termed as "whipping/bending instability", and also due to the use of a planar collector plate.[78,79]

Fong et al.[80] reported that beaded fibers are related to the instability of the polymer jet solution, which strongly depends on the balance between the viscosity and surface tension. The morphology and the effect of the blend ratio on the topological structure of the nanofiber scaffolds can be seen in Figures S3−S5. Once SG/Ch are present in the blend (formulation M2 and M3), there is an increase in bead formation. While with solution M4, a uniform nanofiber morphology was observed, which could be attributed to the viscosity of the solutions. Furthermore, similarly to our rheological results (see Solution Properties section), Gonzalez et al.[81] noticed as the PVA amount decreased beads started to appear in the fibers. This suggests that a decrease in viscosity favors polymer chain disentanglement, which in turn suppresses the spinning process.[62] Furthermore, Figure 4d shows differences in fiber orientation and diameter depending on collector microstructure and viscosity, respectively.

Figure 4c,d shows a smooth and fibrous shape without any bead-like defects. According to Gupta et al.,[82] a reduction in the bead formation can be attributed to an increase in the MW (higher viscosity) because larger polymer chains tend to resist the contraction of the jet radius, which favors the formation of nonbeaded fibers. M4-MP and M4-Flat nanofiber scaffolds have mean fiber diameters of 151 ± 46 and 141 ± 29 nm and surface porosity % of 47 and 46, respectively (see Table 3). Similar to our findings, Tsai et al.[83] reported fiber diameter values of around 150 nm for electrospun Ch−gelatin−PVA hybrid nanofibrous mats, but they did not report the % porosity of the fabricated scaffolds.

SEM micrograph of M4-MP (Figure 4c) shows a nanofiber scaffold with a higher degree of fiber alignment and a relative mean fiber orientation at −48°. Supporting Information (Figure S6) shows M4-MP nanofiber scaffold with different magnifications, which strongly correlates with the designed microstructure topography of the collector plate. On the other hand, Figure 4d shows that M4-Flat does not have a dominant fiber orientation and the polar plot indicates complete randomness with a relative mean fiber orientation ranging between −90 and 90°. It has been proved that aligned scaffolds provide better contact guidance for myoblasts, facilitate cell−cell interactions and cell alignment when compared to random fibers.[26,84,85]

Other authors have published results regarding three-component scaffolds with gelatin, Ch, and PVA as their main components.[83,86] Nevertheless, studies of gelatin/Ch/PVA

https://doi.org/10.1021/acsomega.3c06436
ACS Omega 2023, 8, 47883−47896

continue to be scarce, and furthermore, nanofibers with gelatin from a nonmammalian origin (salmon) have not been used. Therefore, as evidenced by SEM analysis, the resultant SG/Ch/PVA (M4) nanofiber scaffold exhibited better spinnability than just PVA at 10% (w/w) solution (M1), and an aligned fiber orientation, when a MP collector plate is used during electrospinning. We assume the electrospinning process of this blend was possible due to the interaction between PVA with gelatin and Ch molecules through hydrogen bonds, which could weaken the strong interaction of Ch with itself and facilitate the formation of SG/Ch/PVA nanofibers. Finally, it is yet difficult to obtain a perfect nanofiber alignment with this method, given that when the fibers travel from the tip of the needle toward the collector plate, driven by electrostatic forces, the residual charge accumulation on the deposited fibers interferes with the incoming ones, causing an alteration in the alignment and deposition of the nanofibers.[87]

Summarizing, considering the importance of nanofibers as they mimic the aspect of ECM proteins, i.e., ratio and size-scale,[11,88] a MP scaffold with aligned and uniform nanofibers was successfully produced by electrospinning using a SG/Ch/PVA polymer blend.

3.6. Cell Viability Analysis. Biocompatibility of a scaffold is one of the most important prerequisites for biomaterials to satisfy SMTE applications. To evaluate cell viability and behavior of C2C12 cells on SG/Ch/PVA nanofiber scaffolds, a bioluminescence-based assay CellTiter-Glo was assessed, with incubation times of 4, 24, 48, and 72 h. An FPW with DMEM and DMSO 20% were used as positive and negative controls, respectively. The nanofiber scaffolds M1 (Flat and MP) and M4 (Flat and MP) were selected due to their handling and manipulation properties in comparison to the other scaffolds that were fragile and too brittle for this assay (Figure S2). According to the general in vitro cytotoxicity standard ISO 10993-5, to define whether a material is biocompatible, it is important that the value of cell viability be above 70%. In Figure 5, the viability results show that none of the nanofiber scaffolds tested caused cytotoxicity, with cell viability values over 85% compared to the control even after 72 h of incubation.

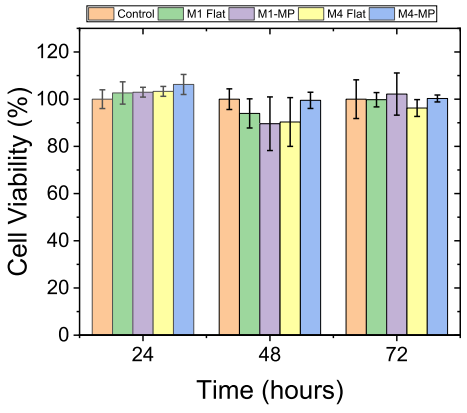

Figure 5. C2C12 viability was determined by the CellTiter-Glo bioluminescent assay. Cell viability of C2C12 cells cultured over SG/Ch/PVA nanofiber scaffolds M1 (Flat and MP) and M4 (Flat and MP) after 4, 24, 48, and 72 h. The bars represent the average of a triplicate and error bars represent the standard deviation (±SD) (n = 4).

After 4 h of incubation with the polymers, a slightly higher viability for the nanofiber scaffold M4-MP compared to M1-MP and the control was observed. Among M4-MP and M1-MP nanofiber scaffolds, the sample M4-MP showed the highest cell viability at 24 h (106%) and equal to the control at 48 h (100%), but slightly lower than M1-MP, 102 and 100% at 72 h of incubation, respectively. PVA has been approved by FDA (U.S. Food and Drug Administration) for clinical uses in humans,[89] thus it was expected that the PVA (M1 Flat and MP) samples were noncytotoxic. Furthermore, the high cell viability values (%) of the SG/Ch/PVA (M4 Flat and MP) nanofiber scaffolds can be associated with the polymer composition and the well-known biocompatibility of each individual component in the blend (SG,[12] Ch,[39] and PVA[49]). Overall, the results shown in Figure 5 demonstrate that all the nanofiber scaffolds produced were noncytotoxic and are suitable for seeding muscle cells. Additionally, this can be correlated with the increase in the luminescence over time, as shown in the cellular behavior assay (Figure 6).

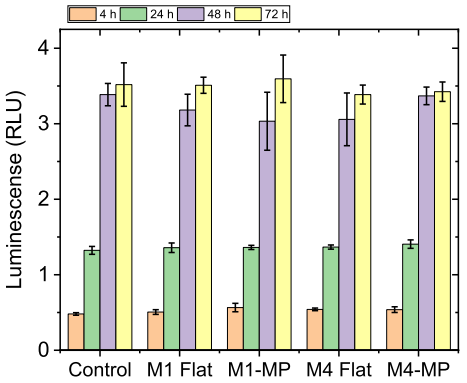

Figure 6. Cellular behavior assay. Luminescence (RLU) was obtained with CellTiter-Glo assay after 4, 24, 48, and 72 h of C2C12 culture over M1 (Flat and MP) and M4 (Flat and MP) nanofiber scaffolds. Results are expressed as the mean luminescence (n = 3) and error bars represent the standard deviation (±SD). No significant differences were found.

Considering the CellTiter-Glo results, there is a linear relationship between the luminescent signal and the number of viable cells per well in culture. As shown in Figure 6, the cell behavior of C2C12 cells over the nanofiber scaffolds M1 (Flat and MP) and M4 (Flat and MP) was assessed up to 72 h. There were no statistical differences between the polymers tested and the FPW with DMEM, indicating that C2C12 cells were able to grow in time over the SG/Ch/PVA nanofiber scaffolds compared to the controls. Therefore, we observe that both composition and microstructure can influence the behavior of the cells.[2,24]

Other authors have reported three-component blends of gelatin, or collagen, Ch and PVA. Most of these studies aim to characterize the blend physically and chemically,[90] its clotting activity for use as wound dressing,[75] the cytocompatibility with mesenchymal stem cells,[83,91] or with human-induced pluripotent stem cells for tissue engineering applications.[86] To the best of our knowledge, there is no other study published over a ternary blend with SG, Ch, and PVA in the form of nanofibers and its biocompatibility with C2C12 cells. Hence, considering our results, the SG/Ch/PVA nanofiber scaffolds produced are biocompatible and could be used for SMTE applications. Nevertheless, future work should be focused on determining

https://doi.org/10.1021/acsomega.3c06436
ACS Omega 2023, 8, 47883−47896

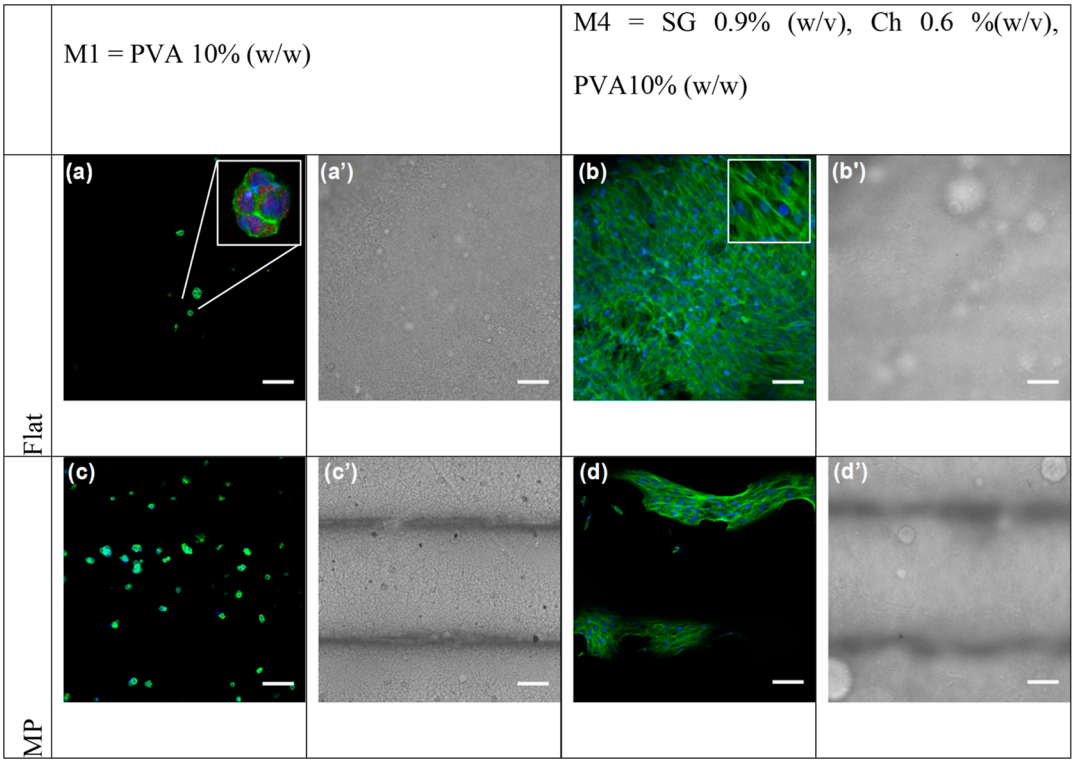

Figure 7. LSCM images of C2C12 cells (green actin filament staining with Rhodamine Phalloidin R415 dye and blue nuclear staining with SYTOX Green dye) cultured for 72 h over the PVA nanofiber scaffolds M1-Flat (a); M1-MP (c); and over SG/Ch/PVA nanofiber scaffolds M4-Flat (b); M4-MP (d). (a′−d′) Bright field microscopy images over the same region of figures (a−d). Scale bar = 100 μm.

whether the MP topography influences cell differentiation on myoblastic cell lines, and many challenges must be overcome in this field to create a suitable SG/Ch/PVA device that meets the requirements to replace a tissue as complex as the skeletal muscle tissue.

3.7. Immunofluorescent Staining. To study cell morphology and investigate the effect of the SG/Ch/PVA nanofiber scaffold microchannels on cell alignment, we imaged the samples using LSCM. C2C12 cells were cultured over SG/Ch/PVA nanofiber scaffolds M1 (Flat and MP) and M4 (Flat and MP). After 72 h of culture, cells were fixed and stained with SYTOX Green for nucleic acid staining (blue) and Rhodamine Phalloidin R415 for actin filament staining (green). As seen from the LSCM images (Figure 7a−d), M4 scaffolds, both Flat and MP, can support growth, adhesion, and spreading of C2C12 cells over the scaffolds. Complementary bright field microscopy images are shown in Figure 7a′−d′.

Pure PVA nanofiber scaffolds (M1 Flat and MP) were easy to handle, biocompatible (see Section 3.6), and had good mechanical stability.[92] Figure 7a,c shows that C2C12 cells have not spread over pure PVA scaffolds (M1) after 72 h and that the cells appear packed, forming round clusters over the nanofiber scaffolds. This could be due to the lack of biological recognition proteins such as RGD motifs, Aα-chain and the heparin binding domain within the Bβ-chain which mediates cell−matrix interactions,[92] and biochemical signals that are inherent to collagen and gelatin polymers. Moreover, PVA by itself does not have a chemical structural similarity to the natural ECM, such as Ch, which is similar to glycosaminoglycans, a class of polysaccharides naturally present in the ECM.[93] Glycosaminoglycans play a key role in cell signaling and are responsible for modulating several biochemical processes, such as regulation of cell growth and proliferation, promotion of cell adhesion, anticoagulation, and wound repair, among others.[94]

Similar results have been previously described regarding the morphology after cells were seeded over PVA scaffolds. Huang and Hu[92] reported how 3T3 fibroblasts appear rounded as grown on PVA fibers. Furthermore, Qi et al.[95] observed that osteoblast cultured on pure PVA scaffolds had a round shape, besides a weak adhesion force with the substrate scaffold. Considering the viability results and LSCM images (Figure 7a,a′ and c,c′) of C2C12 cells over PVA nanofiber scaffolds, cells can grow and proliferate on PVA fibers, but due to the lack of binding proteins and poor cell adhesion properties of the polymer, cell morphology and behavior become compromised.

On the other hand, C2C12 cells over M4 nanofiber scaffolds appear confluent, adhered, spread out, and stretched after 72 h of culture (see Figure 7b,d). These results suggest that the addition of SG on the blend of Ch/PVA has a significant effect on the C2C12 morphology over the nanofiber scaffold. Compared to M1, these results suggest that the presence of biological signals provided by the addition of natural biopolymers (SG and Ch), even at low proportions in a blend, provides physicochemical properties to the matrix, in a way similar to that of the natural ECM, which has a significant effect on C2C12 cell behavior. Cells adhered on the SG/Ch/PVA nanofiber scaffold M4 Flat (Figure 7d) exhibit a random orientation in comparison to M4-MP (Figure 7d′), where cells are oriented alongside the axis of the designed microchannel. Cell orientation is also provided by uniaxially aligned nanofibers that have been shown to increase cell guidance and migration more than randomly organized fibers.

https://doi.org/10.1021/acsomega.3c06436
ACS Omega 2023, 8, 47883−47896

At 72 h of cell culture, cells grow, spread, and exhibit a change in the morphology on both flat and MP M4 scaffolds (Figure 7b,b′−d,d′). Myoblast culture over M4-MP scaffold seemed to be fused and presented an oval and elongated myotube-like morphology oriented in the direction of the microchannel (Figures 7d,d′ and S6a,b). Moreover, the microchannels also allowed the cells to diffuse into the scaffold, as seen in Figure S7c. C2C12 cells were found fused between parallel layers (top, middle, and lower layers) allowing the migration and colonization of cells throughout the nanofiber scaffold. Normally, mouse myoblasts begin to fuse into multinucleated myotubes within 48 h of culture with serum deprivation conditions,[96] but this study was performed without an induced differentiation. Further differentiation experiments need to be performed to determine the expression levels of late myogenic markers, such as myogenin, MyHC, and dystrophin, on muscle cells cultured over SG/Ch/PVA nanofiber scaffolds. Therefore, these results suggest that SG/Ch/PVA nanofiber scaffolds can provide a suitable microenvironment for C2C12 cell growth. Furthermore, the combination of SG/Ch/PVA and the nanofiber organization on the microchannels has proven its synergistic effects for SMTE applications. Future experiments could explore ways of embedding these biopolymers within nanofibers that have additional layers of porosity, which can be generated by thermal sintering techniques.[97,98]

4. CONCLUSIONS

SG/Ch/PVA nanofiber scaffolds were successfully produced by electrospinning using a MP collector. The addition of PVA improved the mechanical and rheological properties of SG and Ch scaffolds. The effect of PVA addition on the handling properties, microstructure, and biocompatibility of M4 SG/Ch/PVA nanofiber scaffolds was studied in detail. Smooth and uniform nanofibers were obtained at an applied voltage of 7 kV and a flow rate of 0.20 mL/h with mean fiber diameters of 151 ± 46 and 141 ± 29 nm for M4 (SG/Ch/PVA MP and flat) and an estimated surface porosity of around 46%.

The viability and cellular behavior assays indicated that SG/Ch/PVA nanofiber scaffolds were suitable for seeding C2C12 cells, allowing the cells to grow over the polymer, possibly due to the similarity between the scaffold topography, nanofiber size, and orientation to those of the natural ECM. On the other hand, C2C12 cells can grow on pure PVA nanofibers (M1), but due to the lack of binding proteins in the polymer, cell morphology and behavior become compromised. MP blended scaffolds (M4-MP) showed enhanced alignment of C2C12 cells and myotube-like formation without an induced differentiation, as compared to randomly oriented fibers. Therefore, C2C12 survival was not dependent on the electrospun fiber diameter, orientation, or scaffold composition.

Blended nanofiber scaffolds from SG, Ch, and PVA are a promising biomaterial for STME-related applications because of its nonzoonotic implications, good biological properties, cytocompatibility, and high availability. This study demonstrates the potential of SG/Ch/PVA MP nanofiber scaffolds. The use of MP collectors for electrospinning is a simple and viable approach to better model skeletal muscle biology in vitro, but further studies need to be performed to probe their suitability in SMTE.

■ ASSOCIATED CONTENT

Supporting Information

The Supporting Information is available free of charge at https://pubs.acs.org/doi/10.1021/acsomega.3c06436.

Schematic illustration of the electrospinning experiment; handling properties of the resulting scaffolds; SEM micrographs of samples M2, M3, and M5; SEM micrographs of sample M4-MP at different magnifications; LSCM of C2C12 cells after 72 h of culture on sample M4-MP; and characteristic FTIR peaks for PVA and CH/SG/PVA blends (PDF)

■ AUTHOR INFORMATION

Corresponding Authors

Cristian A. Acevedo − *Centro de Biotecnología and Centro Científico Tecnológico de Valparaíso (CCTVAL), Universidad Técnica Federico Santa María, Valparaíso 2340000, Chile; Departamento de Física, Universidad Técnica Federico Santa María, Valparaíso 2340000, Chile*; Email: cristian.acevedo@usm.cl

Tomas P. Corrales − *Centro de Biotecnología, Universidad Técnica Federico Santa María, Valparaíso 2340000, Chile; Departamento de Física, Universidad Técnica Federico Santa María, Valparaíso 2340000, Chile; Millenium Nucleus in NanoBioPhysics (NNBP), Valparaíso 2340000, Chile*; orcid.org/0000-0003-0197-9735; Email: tomas.corrales@usm.cl

Authors

María I. Taborda − *Centro de Biotecnología, Universidad Técnica Federico Santa María, Valparaíso 2340000, Chile; Programa de doctorado en Biotecnología, Pontificia Universidad Católica de Valparaíso−Universidad Técnica Federico Santa María, Valparaíso 2340000, Chile*; orcid.org/0000-0001-8636-6852

Karina N. Catalan − *Departamento de Física, Universidad Técnica Federico Santa María, Valparaíso 2340000, Chile*

Nicole Orellana − *Centro de Biotecnología, Universidad Técnica Federico Santa María, Valparaíso 2340000, Chile*

Dragica Bezjak − *Centro de Biotecnología, Universidad Técnica Federico Santa María, Valparaíso 2340000, Chile; Programa de doctorado en Biotecnología, Pontificia Universidad Católica de Valparaíso−Universidad Técnica Federico Santa María, Valparaíso 2340000, Chile*

Javier Enrione − *Escuela de Nutrición y Dietética, Facultad de Medicina, Universidad de los Andes, Las Condes, Santiago 7550000, Chile*

Complete contact information is available at: https://pubs.acs.org/10.1021/acsomega.3c06436

Notes

The authors declare no competing financial interest.

■ ACKNOWLEDGMENTS

The authors thank Dr. Michael Kappl, Dr. Volker Mailänder, Professor Dr. Hans-Jürgen Butt, and their team at the Max Planck Institute for Polymer Research for their support. To the Centro de Biotecnología "Dr. Daniel Alkalay Lowitt" and to all that contributed and collaborated throughout the research. M.I.T. and K.N.C acknowledge financial support from Universidad Técnica Federico Santa María by "Programa de Incentivos a la Iniciación Científica Multidisciplinario"

(PIICM-2018-2). T.P.C. and C.A.A. acknowledge ANID for funding by project Fondecyt Regular 1211901. C.A.A. acknowledges ANID for funding support by projects Fondecyt Regular 1190100 and PIA/APOYO AFB220004. We acknowledge ANID—Millennium Science Initiative Program—NNBP #NCN2021_021 "Millennium Nucleus in NanoBioPhysics".

REFERENCES

(1) Grasman, J. M.; Zayas, M. J.; Page, R. L.; Pins, G. D. Biomimetic Scaffolds for Regeneration of Volumetric Muscle Loss in Skeletal Muscle Injuries. *Acta Biomater.* **2015**, *25*, 2−15.
(2) Mueller, C.; Trujillo-Miranda, M.; Maier, M.; Heath, D. E.; O'Connor, A. J.; Salehi, S. Effects of External Stimulators on Engineered Skeletal Muscle Tissue Maturation. *Adv. Mater. Interfaces* **2021**, *8* (1), 2001167.
(3) Lou, J.; Stowers, R.; Nam, S.; Xia, Y.; Chaudhuri, O. Stress Relaxing Hyaluronic Acid-Collagen Hydrogels Promote Cell Spreading, Fiber Remodeling, and Focal Adhesion Formation in 3D Cell Culture. *Biomaterials* **2018**, *154*, 213−222.
(4) Kuraitis, D.; Giordano, C.; Ruel, M.; Musarò, A.; Suuronen, E. J. Exploiting Extracellular Matrix-Stem Cell Interactions: A Review of Natural Materials for Therapeutic Muscle Regeneration. *Biomaterials* **2012**, *33* (2), 428−443.
(5) Thorsteinsdóttir, S.; Deries, M.; Cachaço, A. S.; Bajanca, F. The Extracellular Matrix Dimension of Skeletal Muscle Development. *Dev. Biol.* **2011**, *354* (2), 191−207.
(6) Brown, B. N.; Badylak, S. F. Extracellular Matrix as an Inductive Scaffold for Functional Tissue Reconstruction. *Transl. Res.* **2014**, *163* (4), 268−285.
(7) Rogers, C. M.; Morris, G. E.; Gould, T. W. A.; Bail, R.; Toumpaniari, S.; Harrington, H.; Dixon, J. E.; Shakesheff, K. M.; Segal, J.; Rose, F. R. A. J. A Novel Technique for the Production of Electrospun Scaffolds with Tailored Three-Dimensional Micro-Patterns Employing Additive Manufacturing. *Biofabrication* **2014**, *6* (3), 035003.
(8) Cittadella Vigodarzere, G.; Mantero, S. Skeletal Muscle Tissue Engineering: Strategies for Volumetric Constructs. *Front. Physiol.* **2014**, *5* DOI: 10.3389/fphys.2014.00362.
(9) Choi, J. S.; Lee, S. J.; Christ, G. J.; Atala, A.; Yoo, J. J. The Influence of Electrospun Aligned Poly(ε-Caprolactone)/Collagen Nanofiber Meshes on the Formation of Self-Aligned Skeletal Muscle Myotubes. *Biomaterials* **2008**, *29* (19), 2899−2906.
(10) Fernández-Costa, J. M.; Fernández-Garibay, X.; Velasco-Mallorquí, F.; Ramón-Azcón, J. Bioengineered in Vitro Skeletal Muscles as New Tools for Muscular Dystrophies Preclinical Studies. *J. Tissue Eng.* **2021**, *12*, 2041731420981339.
(11) Jana, S.; Levengood, S. K. L.; Zhang, M. Anisotropic Materials for Skeletal-Muscle-Tissue Engineering. *Adv. Mater.* **2016**, *28* (48), 10588−10612.
(12) Acevedo, C. A.; Orellana, N.; Avarias, K.; Ortiz, R.; Benavente, D.; Prieto, P. Micropatterning Technology to Design an Edible Film for In Vitro Meat Production. *Food Bioprocess Technol.* **2018**, *11* (7), 1267−1273.
(13) Denes, L. T.; Riley, L. A.; Mijares, J. R.; Arboleda, J. D.; McKee, K.; Esser, K. A.; Wang, E. T. Culturing C2C12 Myotubes on Micromolded Gelatin Hydrogels Accelerates Myotube Maturation. *Skeletal Muscle* **2019**, *9* (1), 17.
(14) Sun, Y.; Duffy, R.; Lee, A.; Feinberg, A. W. Optimizing the Structure and Contractility of Engineered Skeletal Muscle Thin Films. *Acta Biomater.* **2013**, *9* (8), 7885−7894.
(15) Duffy, R. M.; Sun, Y.; Feinberg, A. W. Understanding the Role of ECM Protein Composition and Geometric Micropatterning for Engineering Human Skeletal Muscle. *Ann. Biomed Eng.* **2016**, *44* (6), 2076−2089.
(16) Hwang, Y.; Seo, T.; Hariri, S.; Choi, C.; Varghese, S. Matrix Topographical Cue-Mediated Myogenic Differentiation of Human Embryonic Stem Cell Derivatives. *Polymers* **2017**, *9* (11), 580.
(17) Lee, H.; Kim, W.; Lee, J.; Yoo, J. J.; Kim, G. H.; Lee, S. J. Effect of Hierarchical Scaffold Consisting of Aligned DECM Nanofibers and Poly(Lactide-Co-Glycolide) Struts on the Orientation and Maturation of Human Muscle Progenitor Cells. *ACS Appl. Mater. Interfaces* **2019**, *11* (43), 39449−39458.
(18) Golba, B.; Kalaoglu-Altan, O. I.; Sanyal, R.; Sanyal, A. Hydrophilic Cross-Linked Polymeric Nanofibers Using Electrospinning: Imparting Aqueous Stability to Enable Biomedical Applications. *ACS Appl. Polym. Mater.* **2021**, *4* (1), 1−17.
(19) Ewaldz, E.; Brettmann, B. Molecular Interactions in Electrospinning: From Polymer Mixtures to Supramolecular Assemblies. *ACS Appl. Polym. Mater.* **2019**, *1* (3), 298−308.
(20) Zhang, D.; Chang, J. Electrospinning of Three-Dimensional Nanofibrous Tubes with Controllable Architectures. *Nano Lett.* **2008**, *8* (10), 3283−3287.
(21) Wang, Y.; Shi, H.; Qiao, J.; Tian, Y.; Wu, M.; Zhang, W.; Lin, Y.; Niu, Z.; Huang, Y. Electrospun Tubular Scaffold with Circumferentially Aligned Nanofibers for Regulating Smooth Muscle Cell Growth. *ACS Appl. Mater. Interfaces* **2014**, *6* (4), 2958−2962.
(22) Jia, L.; Prabhakaran, M. P.; Qin, X.; Ramakrishna, S. Guiding the Orientation of Smooth Muscle Cells on Random and Aligned Polyurethane/Collagen Nanofibers. *J. Biomater. Appl.* **2014**, *29* (3), 364−377.
(23) Jin, G.; He, R.; Sha, B.; Li, W.; Qing, H.; Teng, R.; Xu, F. Electrospun Three-Dimensional Aligned Nanofibrous Scaffolds for Tissue Engineering. *Mater. Sci. Eng.* **2018**, *92*, 995−1005.
(24) Jun, I.; Han, H. S.; Edwards, J. R.; Jeon, H. Electrospun Fibrous Scaffolds for Tissue Engineering: Viewpoints on Architecture and Fabrication. *Int. J. Mol. Sci.* **2018**, *19*, 745 MDPI AG March 6.
(25) Wang, Z.; Cui, W. Two Sides of Electrospun Fiber in Promoting and Inhibiting Biomedical Processes. *Adv. Ther.* **2021**, *4* (1), 2000096.
(26) Narayanan, N.; Jiang, C.; Wang, C.; Uzunalli, G.; Whittern, N.; Chen, D.; Jones, O. G.; Kuang, S.; Deng, M. Harnessing Fiber Diameter-Dependent Effects of Myoblasts Toward Biomimetic Scaffold-Based Skeletal Muscle Regeneration. *Front. Bioeng. Biotechnol.* **2020**, *8*, 203.
(27) Sirivisoot, S.; Harrison, B. S. Skeletal Myotube Formation Enhanced by Electrospun Polyurethane Carbon Nanotube Scaffolds. *Int. J. Nanomed.* **2011**, *6*, 2483−2497.
(28) Apsite, I.; Uribe, J. M.; Posada, A. F.; Rosenfeldt, S.; Salehi, S.; Ionov, L. 4D Biofabrication of Skeletal Muscle Microtissues. *Biofabrication* **2020**, *12* (1), 015016.
(29) Takeda, N.; Tamura, K.; Mineguchi, R.; Ishikawa, Y.; Haraguchi, Y.; Shimizu, T.; Hara, Y. In Situ Cross-Linked Electrospun Fiber Scaffold of Collagen for Fabricating Cell-Dense Muscle Tissue. *J. Artif. Organs* **2016**, *19* (2), 141−148.
(30) Perez-Puyana, V.; Wieringa, P.; Yuste, Y.; de la Portilla, F.; Guererro, A.; Romero, A.; Moroni, L. Fabrication of Hybrid Scaffolds Obtained from Combinations of PCL with Gelatin or Collagen via Electrospinning for Skeletal Muscle Tissue Engineering. *J. Biomed. Mater. Res., Part A* **2021**, *109* (9), 1600−1612.
(31) Somers, S. M.; Zhang, N. Y.; Morrissette-McAlmon, J. B. F.; Tran, K.; Mao, H.-Q.; Grayson, W. L. Myoblast Maturity on Aligned Microfiber Bundles at the Onset of Strain Application Impacts Myogenic Outcomes. *Acta Biomater.* **2019**, *94*, 232−242.
(32) Wang, L.; Wu, Y.; Guo, B.; Ma, P. X. Nanofiber Yarn/Hydrogel Core-Shell Scaffolds Mimicking Native Skeletal Muscle Tissue for Guiding 3D Myoblast Alignment, Elongation, and Differentiation. *ACS Nano* **2015**, *9* (9), 9167−9179.
(33) Cooper, A.; Jana, S.; Bhattarai, N.; Zhang, M. Aligned Chitosan-Based Nanofibers for Enhanced Myogenesis. *J. Mater. Chem.* **2010**, *20* (40), 8904−8911.
(34) Kheradmandi, M.; Vasheghani-Farahani, E.; Ghiaseddin, A.; Ganji, F. Skeletal Muscle Regeneration via Engineered Tissue Culture over Electrospun Nanofibrous Chitosan/PVA Scaffold. *J. Biomed. Mater. Res., Part A* **2016**, *104* (7), 1720−1727.
(35) Lapomarda, A.; Degli Esposti, M.; Micalizzi, S.; Fabbri, P.; Raspolli Galletti, A. M.; Morselli, D.; De Maria, C. Valorization of a

https://doi.org/10.1021/acsomega.3c06436
ACS Omega 2023, 8, 47883−47896

Levulinic Acid Platform through Electrospinning of Polyhydroxyalkanoate-Based Fibrous Membranes for In Vitro Modeling of Biological Barriers. *ACS Appl. Polym. Mater.* **2022**, *4* (8), 5872−5881.
(36) Liguori, A.; Uranga, J.; Panzavolta, S.; Guerrero, P.; de la Caba, K.; Focarete, M. L. Electrospinning of Fish Gelatin Solution Containing Citric Acid: An Environmentally Friendly Approach to Prepare Crosslinked Gelatin Fibers. *Materials* **2019**, *12* (17), 2808.
(37) Enrione, J.; Blaker, J. J.; Brown, D. I.; Weinstein-Oppenheimer, C. R.; Pepczynska, M.; Olguín, Y.; Sánchez, E.; Acevedo, C. A. Edible Scaffolds Based on Non-Mammalian Biopolymers for Myoblast Growth. *Materials* **2017**, *10* (12), 1404.
(38) Acevedo, C. A.; Olguín, Y.; Orellana, N.; Sánchez, E.; Pepczynska, M.; Enrione, J. Anatase Incorporation to Bioactive Scaffolds Based on Salmon Gelatin and Its Effects on Muscle Cell Growth. *Polymers* **2020**, *12* (9), 1943.
(39) Enrione, J.; Pino, K.; Pepczynska, M.; Brown, D. I.; Ortiz, R.; Sánchez, E.; Acevedo, C. A. A Novel Biomaterial Based on Salmon-Gelatin and Its in Vivo Evaluation as Sterile Wound-Dressing. *Mater. Lett.* **2018**, *212*, 159−164.
(40) Amiri, N.; Rozbeh, Z.; Afrough, T.; Sajadi Tabassi, S. A.; Moradi, A.; Movaffagh, J. Optimization of Chitosan-Gelatin Nanofibers Production: Investigating the Effect of Solution Properties and Working Parameters on Fibers Diameter. *Bionanoscience* **2018**, *8* (3), 778−789.
(41) Yamada, S.; Yamamoto, K.; Ikeda, T.; Yanagiguchi, K.; Hayashi, Y. Potency of Fish Collagen as a Scaffold for Regenerative Medicine. *Biomed. Res. Int.* **2014**, *2014*, 1−8.
(42) Hsu, H.-H.; Uemura, T.; Yamaguchi, I.; Ikoma, T.; Tanaka, J. Chondrogenic Differentiation of Human Mesenchymal Stem Cells on Fish Scale Collagen. *J. Biosci. Bioeng.* **2016**, *122* (2), 219−225.
(43) Hassanbhai, A. M.; Lau, C. S.; Wen, F.; Jayaraman, P.; Goh, B. T.; Yu, N.; Teoh, S.-H. In Vivo Immune Responses of Cross-Linked Electrospun Tilapia Collagen Membrane. *Tissue Eng., Part A* **2017**, *23* (19−20), 1110−1119.
(44) Ahmed, S.; Ikram, S. Chitosan Based Scaffolds and Their Applications in Wound Healing. *Achiev. Life Sci.* **2016**, *10* (1), 27−37.
(45) Ullah, S.; Zainol, I.; Chowdhury, S. R.; Fauzi, M. B. Development of Various Composition Multicomponent Chitosan/Fish Collagen/Glycerin 3D Porous Scaffolds: Effect on Morphology, Mechanical Strength, Biostability and Cytocompatibility. *Int. J. Biol. Macromol.* **2018**, *111*, 158−168.
(46) Li, Q.; Wang, X.; Lou, X.; Yuan, H.; Tu, H.; Li, B.; Zhang, Y. Genipin-Crosslinked Electrospun Chitosan Nanofibers: Determination of Crosslinking Conditions and Evaluation of Cytocompatibility. *Carbohydr. Polym.* **2015**, *130*, 166−174.
(47) Fathollahipour, S.; Abouei Mehrizi, A.; Ghaee, A.; Koosha, M. Electrospinning of PVA/Chitosan Nanocomposite Nanofibers Containing Gelatin Nanoparticles as a Dual Drug Delivery System. *J. Biomed. Mater. Res., Part A* **2015**, *103* (12), 3852−3862.
(48) Chiellini, E.; Corti, A.; D'Antone, S.; Solaro, R. Biodegradation of Poly (Vinyl Alcohol) Based Materials. *Prog. Polym. Sci.* **2003**, *28* (6), 963−1014.
(49) Zulkiflee, I.; Fauzi, M. B. Gelatin-Polyvinyl Alcohol Film for Tissue Engineering: A Concise Review. *Biomedicines* **2021**, *9*, 979 MDPI AG August 1.
(50) Jin, S. G. Production and Application of Biomaterials Based on Polyvinyl Alcohol (PVA) as Wound Dressing. *Chem.—Asian J.* **2022**, *17* (21), No. e202200595.
(51) Rivera-Hernández, G.; Antunes-Ricardo, M.; Martínez-Morales, P.; Sánchez, M. L. Polyvinyl Alcohol Based-Drug Delivery Systems for Cancer Treatment. *Int. J. Pharm.* **2021**, *600*, 120478.
(52) Hotaling, N. A.; Bharti, K.; Kriel, H.; Simon, C. G. DiameterJ: A Validated Open Source Nanofiber Diameter Measurement Tool. *Biomaterials* **2015**, *61*, 327−338.
(53) Hotaling, N. A.; Bharti, K.; Kriel, H.; Simon, C. G. Dataset for the Validation and Use of DiameterJ an Open Source Nanofiber Diameter Measurement Tool. *Data Brief* **2015**, *5*, 13−22.
(54) Bhattarai, N.; Edmondson, D.; Veiseh, O.; Matsen, F. A.; Zhang, M. Electrospun Chitosan-Based Nanofibers and Their Cellular Compatibility. *Biomaterials* **2005**, *26* (31), 6176−6184.
(55) Alfaro, A. d. T.; Balbinot, E.; Weber, C. I.; Tonial, I. B.; Machado-Lunkes, A. Fish Gelatin: Characteristics, Functional Properties, Applications and Future Potentials. *Food Eng. Rev.* **2015**, *7* (1), 33−44.
(56) Acevedo, C. A.; Díaz-Calderón, P.; López, D.; Enrione, J. Assessment of Gelatin-Chitosan Interactions in Films by a Chemometrics Approach. *CyTA—J. Food* **2015**, *13* (2), 227−234.
(57) Gómez-Guillén, M.; Pérez-Mateos, M.; Gómez-Estaca, J.; López-Caballero, E.; Giménez, B.; Montero, P. Fish Gelatin: A Renewable Material for Developing Active Biodegradable Films. *Trends Food Sci. Technol.* **2009**, *20* (1), 3−16.
(58) Ghaderi, J.; Hosseini, S. F.; Keyvani, N.; Gómez-Guillén, M. C. Polymer Blending Effects on the Physicochemical and Structural Features of the Chitosan/Poly(Vinyl Alcohol)/Fish Gelatin Ternary Biodegradable Films. *Food Hydrocolloids* **2019**, *95*, 122−132.
(59) Balagangadharan, K.; Dhivya, S.; Selvamurugan, N. Chitosan Based Nanofibers in Bone Tissue Engineering. *Int. J. Biol. Macromol.* **2017**, *104*, 1372−1382.
(60) Ranganathan, S.; Balagangadharan, K.; Selvamurugan, N. Chitosan and Gelatin-Based Electrospun Fibers for Bone Tissue Engineering. *Int. J. Biol. Macromol.* **2019**, *133*, 354−364.
(61) Palazzi, F.; Morra, M.; Mohammadi, Z.; Grandini, S.; Giardino, L. Comparison of the Surface Tension of 5.25% Sodium Hypochlorite Solution with Three New Sodium Hypochlorite-Based Endodontic Irrigants. *Int. Endod. J.* **2012**, *45* (2), 129−135.
(62) Rwei, S.-P.; Huang, C.-C. Electrospinning PVA Solution-Rheology and Morphology Analyses. *Fibers Polym.* **2012**, *13* (1), 44−50.
(63) Rošic, R.; Pelipenko, J.; Kristl, J.; Kocbek, P.; Bešter-Rogač, M.; Baumgartner, S. Physical Characteristics of Poly (Vinyl Alcohol) Solutions in Relation to Electrospun Nanofiber Formation. *Eur. Polym. J.* **2013**, *49* (2), 290−298.
(64) Elsabee, M. Z.; Naguib, H. F.; Morsi, R. E. Chitosan Based Nanofibers, Review. *Mater. Sci. Eng., C* **2012**, *32* (7), 1711−1726.
(65) Andrade, G.; Barbosa-Stancioli, E. F.; Mansur, A. A. P.; Vasconcelos, W. L.; Mansur, H. S. Design of Novel Hybrid Organic-Inorganic Nanostructured Biomaterials for Immunoassay Applications. *Biomed. Mater.* **2006**, *1* (4), 221−234.
(66) Mansur, H. S.; Sadahira, C. M.; Souza, A. N.; Mansur, A. A. P. FTIR Spectroscopy Characterization of Poly (Vinyl Alcohol) Hydrogel with Different Hydrolysis Degree and Chemically Crosslinked with Glutaraldehyde. *Mater. Sci. Eng., C* **2008**, *28* (4), 539−548.
(67) Andrade, G. I.; Barbosa-Stancioli, E. F.; Mansur, A. A. P.; Vasconcelos, W. L.; Mansur, H. S. Small-Angle X-Ray Scattering and FTIR Characterization of Nanostructured Poly (Vinyl Alcohol)/Silicate Hybrids for Immunoassay Applications. *J. Mater. Sci.* **2008**, *43* (2), 450−463.
(68) Acevedo, C. A.; Sánchez, E.; Díaz-Calderón, P.; Blaker, J. J.; Enrione, J.; Quero, F. Synergistic Effects of Crosslinking and Chitosan Molecular Weight on the Microstructure, Molecular Mobility, Thermal and Sorption Properties of Porous Chitosan/Gelatin/Hyaluronic Acid Scaffolds. *J. Appl. Polym. Sci.* **2017**, *134*, 44772.
(69) Wang, X. H.; Li, D. P.; Wang, W. J.; Feng, Q. L.; Cui, F. Z.; Xu, Y. X.; Song, X. H.; Van Der Werf, M. Crosslinked Collagen/Chitosan Matrix for Artificial Livers. *Biomaterials* **2003**, *24* (19), 3213−3220.
(70) Parida, U. K.; Nayak, A. K.; Binhani, B. K.; Nayak, P. L. Synthesis and Characterization of Chitosan-Polyvinyl Alcohol Blended with Cloisite 30B for Controlled Release of the Anticancer Drug Curcumin. *J. Biomater. Nanobiotechnol.* **2011**, *02*, 414−425.
(71) Staroszczyk, H.; Sztuka, K.; Wolska, J.; Wojtasz-Pająk, A.; Kołodziejska, I. Interactions of Fish Gelatin and Chitosan in Uncrosslinked and Crosslinked with EDC Films: FT-IR Study. *Spectrochim. Acta, Part A* **2014**, *117*, 707−712.
(72) de Souza Costa-Júnior, E.; Pereira, M. M.; Mansur, H. S. Properties and Biocompatibility of Chitosan Films Modified by

https://doi.org/10.1021/acsomega.3c06436
ACS Omega 2023, 8, 47883−47896

Blending with PVA and Chemically Crosslinked. *J. Mater. Sci.: Mater. Med.* **2009**, *20* (2), 553−561.
(73) Taravel, M. N.; Domard, A. Collagen and Its Interaction with Chitosan: II. Influence of the Physicochemical Characteristics of Collagen. *Biomaterials* **1995**, *16* (11), 865−871.
(74) Krishna Rao, K. S. V.; Vijaya Kumar Naidu, B.; Subha, M. C. S.; Sairam, M.; Aminabhavi, T. M. Novel Chitosan-Based PH-Sensitive Interpenetrating Network Microgels for the Controlled Release of Cefadroxil. *Carbohydr. Polym.* **2006**, *66* (3), 333−344.
(75) Fan, L.; Yang, H.; Yang, J.; Peng, M.; Hu, J. Preparation and Characterization of Chitosan/Gelatin/PVA Hydrogel for Wound Dressings. *Carbohydr. Polym.* **2016**, *146*, 427−434.
(76) Park, J.-C.; Ito, T.; Kim, K.-O.; Kim, K.-W.; Kim, B.-S.; Khil, M.-S.; Kim, H.-Y.; Kim, I.-S. Electrospun Poly(Vinyl Alcohol) Nanofibers: Effects of Degree of Hydrolysis and Enhanced Water Stability. *Polym. J.* **2010**, *42* (3), 273−276.
(77) Zhang, C.; Yuan, X.; Wu, L.; Han, Y.; Sheng, J. Study on Morphology of Electrospun Poly(Vinyl Alcohol) Mats. *Eur. Polym. J.* **2005**, *41* (3), 423−432.
(78) Ali, U.; Zhou, Y.; Wang, X.; Lin, T. Electrospinning of Continuous Nanofiber Bundles and Twisted Nanofiber Yarns. In *Nanofibers*; Lin, T., Ed.; IntechOpen: Rijeka, 2011, Chapter 8..
(79) Asmatulu, R.; Khan, W. S. Historical Background of the Electrospinning Process. *Synthesis and Applications of Electrospun Nanofibers*; Elsevier, 2019; pp 17−39..
(80) Fong, H.; Chun, I.; Reneker, D. H. Beaded Nanofibers Formed during Electrospinning. *Polymer* **1999**, *40* (16), 4585−4592.
(81) Gonzalez, E.; Barquero, A.; Muñoz-sanchez, B.; Paulis, M.; Leiza, J. R. Green Electrospinning of Polymer Latexes: A Systematic Study of the Effect of Latex Properties on Fiber Morphology. *Nanomaterials* **2021**, *11* (3), 706.
(82) Gupta, P.; Elkins, C.; Long, T. E.; Wilkes, G. L. Electrospinning of Linear Homopolymers of Poly(Methyl Methacrylate): Exploring Relationships between Fiber Formation, Viscosity, Molecular Weight and Concentration in a Good Solvent. *Polymer* **2005**, *46* (13), 4799−4810.
(83) Tsai, R. Y.; Hung, S. C.; Lai, J. Y.; Wang, D. M.; Hsieh, H. J. Electrospun Chitosan-Gelatin-Polyvinyl Alcohol Hybrid Nanofibrous Mats: Production and Characterization. *J. Taiwan Inst. Chem. Eng.* **2014**, *45* (4), 1975−1981.
(84) Aviss, K. J.; Gough, J. E.; Downes, S. Aligned Electrospun Polymer Fibres for Skeletal Muscle Regeneration. *Eur. Cells Mater.* **2010**, *19*, 193−204.
(85) Zhang, Y.; Lei, Y.; Chang, J.; Li, L.; He, B.; Gu, Z. Guidance of Myoblast Migration on Aligned Electrospun PLGA Nanofibrous Meshes. *Mater. Lett.* **2012**, *68*, 218−221.
(86) Mokhames, Z.; Rezaie, Z.; Ardeshirylajimi, A.; Basiri, A.; Taheri, M.; Omrani, M. D. Efficient Smooth Muscle Cell Differentiation of IPS Cells on Curcumin-Incorporated Chitosan/Collagen/Polyvinyl-Alcohol Nanofibers. *In Vitro Cell. Dev. Biol.: Anim.* **2020**, *56* (4), 313−321.
(87) Robinson, A. J.; Pérez-Nava, A.; Ali, S. C.; González-Campos, J. B.; Holloway, J. L.; Cosgriff-Hernandez, E. M. Comparative Analysis of Fiber Alignment Methods in Electrospinning. *Matter* **2021**, *4* (3), 821−844.
(88) Ostrovidov, S.; Hosseini, V.; Ahadian, S.; Fujie, T.; Parthiban, S. P.; Ramalingam, M.; Bae, H.; Kaji, H.; Khademhosseini, A. Skeletal Muscle Tissue Engineering: Methods to Form Skeletal Myotubes and Their Applications. *Tissue Eng., Part B* **2014**, *20* (5), 403−436.
(89) Chong, S.-F.; Smith, A. A. A.; Zelikin, A. N. Microstructured, Functional PVA Hydrogels through Bioconjugation with Oligopeptides under Physiological Conditions. *Small* **2013**, *9* (6), 942−950.
(90) Al-Mofty, S. E. D.; Karaly, A. H.; Sarhan, W. A.; Azzazy, H. M. E. Multifunctional Hemostatic PVA/Chitosan Sponges Loaded with Hydroxyapatite and Ciprofloxacin. *ACS Omega* **2022**, *7* (15), 13210−13220.
(91) Tsai, R. Y.; Kuo, T. Y.; Hung, S. C.; Lin, C. M.; Hsien, T. Y.; Wang, D. M.; Hsieh, H. J. Use of Gum Arabic to Improve the Fabrication of Chitosan-Gelatin-Based Nanofibers for Tissue Engineering. *Carbohydr. Polym.* **2015**, *115*, 525−532.
(92) Huang, C.-Y.; Hu, K.-H.; Wei, Z.-H. Comparison of Cell Behavior on Pva/Pva-Gelatin Electrospun Nanofibers with Random and Aligned Configuration. *Sci. Rep.* **2016**, *6* (1), 37960.
(93) Nicolas, J.; Magli, S.; Rabbachin, L.; Sampaolesi, S.; Nicotra, F.; Russo, L. 3D Extracellular Matrix Mimics: Fundamental Concepts and Role of Materials Chemistry to Influence Stem Cell Fate. *Biomacromolecules* **2020**, *21* (6), 1968−1994.
(94) Kim, C.-H.; Park, S. J.; Yang, D. H.; Chun, H. J. Chitosan for Tissue Engineering. In *Novel Biomaterials for Regenerative Medicine*; Chun, H. J., Park, K., Kim, C.-H., Khang, G., Eds.; Springer Singapore: Singapore, 2018; pp 475−485..
(95) Qi, Y. Y.; Tai, Z. X.; Sun, D. F.; Chen, J. T.; Ma, H. B.; Yan, X. B.; Liu, B.; Xue, Q. J. Fabrication and Characterization of Poly(Vinyl Alcohol)/Graphene Oxide Nanofibrous Biocomposite Scaffolds. *J. Appl. Polym. Sci.* **2013**, *127* (3), 1885−1894.
(96) White, J.; Barro, M. V.; Makarenkova, H. P.; Sanger, J. W.; Sanger, J. M. Localization of Sarcomeric Proteins During Myofibril Assembly in Cultured Mouse Primary Skeletal Myotubes. *Anat. Rec.* **2014**, *297* (9), 1571−1584.
(97) Friedemann, K.; Corrales, T.; Kappl, M.; Landfester, K.; Crespy, D. Facile and Large-Scale Fabrication of Anisometric Particles from Fibers Synthesized by Colloid-Electrospinning. *Small* **2012**, *8* (1), 144−153.
(98) Corrales, T. P.; Friedemann, K.; Fuchs, R.; Roy, C.; Crespy, D.; Kappl, M. Breaking Nano-Spaghetti: Bending and Fracture Tests of Nanofibers. *Langmuir* **2016**, *32* (5), 1389−1395.

https://doi.org/10.1021/acsomega.3c06436
ACS Omega 2023, 8, 47883−47896